Cambridge Centre for Computational Chemical Engineering

University of Cambridge

Department of Chemical Engineering

Preprint ISSN 1473 – 4273

Applying response surface methodology to multidimensional granulation modelling

Andreas Braumann [1] , Markus Kraft [1] , Paul R. Mort [2]

released: 1 May 2008

[1] Department of Chemical Engineering
University of Cambridge
New Museums Site
Pembroke Street
Cambridge, CB2 3RA
UK
E-mail: mk306@cam.ac.uk

[2] Procter and Gamble Co.
ITC
5299 Spring Grove Avenue
Cincinnati
OH 45217
USA

Preprint No. 56

c4e

Key words and phrases: granulation, agglomeration, modelling, multidimensional population balance, response surface methodology

Edited by
Cambridge Centre for Computational Chemical Engineering
Department of Chemical Engineering
University of Cambridge
Cambridge CB2 3RA
United Kingdom.

Fax: + 44 (0)1223 334796
E-Mail: c4e@cheng.cam.ac.uk
World Wide Web: http://www.cheng.cam.ac.uk/c4e/

Abstract

A new multidimensional model for the wet granulation of powders is presented, which includes the transformations coalescence, compaction, reaction, penetration and breakage. The particles and their composition are described by six dimensions. The particle model consists of two kinds of solid (original and reacted), pore volume, two kinds of liquid (on the external surface and in the pores) and the number of entities (beads) in the particle. This allows for a detailed tracking of the granulation process. Process operating conditions such as the impeller speed of the mixer and the binder composition are reflected in the descriptions of the transformations. The model framework is tested against experimental results (Simmons, Turton and Mort. Proceedings of Fifth World Congress on Particle Technology, paper 9d, 2006) from granulation of sugar particles with different PEG based binders in a bench scale mixer. The experiments were carried out for different impeller speeds, binder compositions and process durations. A response surface approach is chosen in order to establish important model parameters of the subprocesses incorporated in the model through an optimisation step, fitting the model to the set of experiments. These model parameters are the collision rate constant, the compaction rate constant, breakage rate constant, and the reaction rate constant. The simulations with this set of parameters show that the model predicts the correct trends, not only in time, but also for crucial process conditions such as the impeller speed and the binder composition. The influence of their choice is discussed for the porosity of the particle ensemble that is linked to important macro properties like the dissolution behaviour and bulk density. Furthermore, statistics of the different events such as collisions, coalescence and breakage reveal which processes are governing the granulation at different stages under varying conditions. For instance, it has been found that successful coalescence events outnumber the breakage events by a factor of up to three for low impeller speeds.

Contents

1 Introduction

Although granulation or agglomeration processes have been performed on industrial scales for decades, they have not yet been fully understood. Granules are produced in various industries for a wide range of products. Such granules can either be used by other industries, e. g. fertilizer and ore pellets, or private consumers, e. g. washing powders and drugs. In the latter case granules are often not visible to the user as they are embedded in tablets or dragées.

All of these granulation processes have in common that the products need to fulfil specific quality requirements in order to serve for the desired use. The creation of desirable particulate material can either be achieved via dry granulation or by wet granulation (e. g. in fluidized beds, rotating drums or high shear mixers [28]). In the latter case the solid-liquid-ratio plays a crucial role as the liquid acts as mediator between the solid particles and promotes the growth/build up of granules. In various studies, so called regime maps have been established [11, 13, 15]. Although these maps describe very well what can be observed in a granulator (crumbling, steady growth, etc.) under different conditions, they do not solve the questions about the underlying mechanisms completely.

If a granule is observed on the microlevel, several subprocesses can be distinguished. There is no dispute in the community that granulation is governed by coalescence (including layering) and breakage (attrition and fragmentation) [14]. As liquid is part of the system as well, it is important how the liquid (binder) is added, whether it is sprayed into the vessel [1] or put in as a paste (melt binder) [23]. The growth process of the granules is then influenced by the spreading, i. e. the distribution of the binder. Spreading is, among others factors, governed by the droplet size, spray rate, powder bed movements and penetration of the liquid [10, 32]. The interaction of all these processes will determine the behaviour of the system and the outcome of the granulation process. The linking of the different subprocesses is sketched in fig. 1. Through the addition of binder the particles are wetted. After picking up some binder the particles start to coalesce/grow. Due to impacts experienced in the equipment (e. g. from the impeller) the particles will then undergo consolidation, also known as compaction. Depending on the material properties and the process conditions breakage of the granules will occur, causing the disintegration

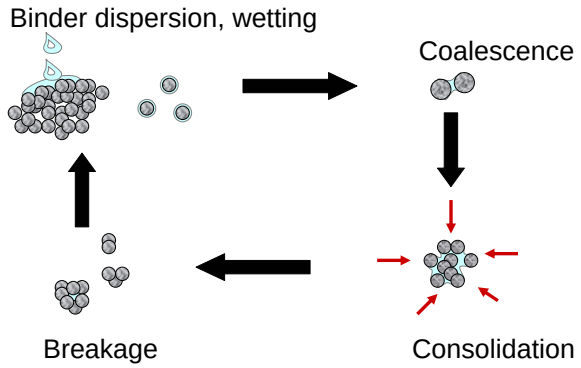

Figure 1: *Stages of a wet granulation process*

of the granules. However, the breakage of the wet particles leads also to the dispersion of the binder, so that the liquid component is spread throughout the particle ensemble enabling further coalescence events. Although coalescence and breakage are antagonistic processes, both are necessary to drive the granulation process. The question is: which ratio of coalescence to breakage events is most beneficial to the overall process?

As all the influences mentioned above have an impact on the performance of (industrial) granulation processes, it would be beneficial to have a very good understanding of the process in order to use certain process variables (e. g. flowrate of binder, droplet size, impeller speed) as control variables so that the process can be controlled [6].

If model predictive control is used, a well suited model of the process is necessary in order to get the best handle on the process. Modelling of granulation processes is done with population balances, which are also used in other fields ranging from combustion (soot formation) [25, 26] and crystallisation [7] to liquid-liquid extraction [9]. For granulation it started in the 60's with one dimension [17]. But it turned out that it is necessary to incorporate more than one dimension [12] in order to keep track of the several components in a granule. In recent work a model framework with five dimensions has been proposed [2]. Such a complex model contains quite a few process variables and parameters. By varying a set of variables within a given range, it is possible to assess the sensitivities of the process. Experimental design, as this mapping is called, allows us to study the effects of the variables considered. It is then possible to identify optimal process conditions [31]. However, the number of levels for each variable in the experimental design is normally kept low (usually two or three). This means, for the evaluation of the process response in the entire range, one has to use a continuous mapping. For instance, it is possible to construct a response surface based on the results of the experimental design.

The **purpose of this paper** is to employ a response surface methodology approach to an extended wet granulation model based on [2]. This existing model is modified in such a way that changes in process conditions such as impeller speed and binder composition, and hence the binder viscosity, are reflected in the various transformations. The new multidimensional model includes the transformations coalescence, compaction, reaction, penetration and breakage. The response surface methodology approach is then employed in order to establish a set of process independent model parameters on the basis of a set of experimental data from [24]. The sensitivity of the model with respect to certain process conditions is tested with the derived set of model parameters. The influence of the process conditions on the porosity of the particles as an important property is also discussed. Furthermore, statistics of the different events such as collisions, coalescence and breakage are presented in order to find out which processes govern the granulation at different stages and under varying conditions.

2 Experimental background

The current paper is inspired by a previous experimental study [24] that investigated the effects of binder composition and mixing rate on the liquid spreading over time. In these experiments sugar particles of a fairly narrow size class were used as solid material being mixed with different mixtures of water and PEG4000 in a standard Braun mixer (model:

K600 CombiMax).

Amongst other characteristics the mass of agglomerates was determined for various parameter sets and times. The results of these measurements are summarised in table 1. Several trends can be observed in these data. For a fixed impeller speed and a binder with a water/PEG4000 ratio of 50:50 the mass of agglomerates decreases monotonically over time for any of the chosen impeller speeds. Also it is noticeable that the mass of agglomerates at the final time $t = 80\,\mathrm{s}$ reduces with an increasing amount of water in the binder for a given impeller speed. Although the data suggest such trends, it has to be mentioned that the value for an impeller speed of 900 rpm and a binder with a water/PEG4000 ratio of 70:30 does not quite follow the trend. Furthermore the mass of agglomerates decreases with increasing impeller speed for any time and any binder composition.

3 Process modelling

The aforementioned granulation process shall be modelled in the forthcoming section. A common way for such modelling work is the use of population balance equations which describe the evolution of the particle ensemble over time. For a complete description of the process one must define which properties of the particles are being tracked in the population balance, which transformations these particles can undergo, and with which rates these transformations happen.

In this section we present an improved model framework building upon a previous five-dimensional granulation model [2]. The new model makes use of a six-dimensional state space. In addition to this, attention is paid to the incorporation of the operating conditions such as the impeller speed of the mixer in the rate laws of the various transformations. These are also dependent on the binder composition and hence the binder viscosity.

3.1 State space

Granules often consist of many components. As has been shown previously [12], the composition of a granule has to be taken into account in order to obtain a satisfying description of the granulation process.

Previous work [2] proposed a particle description with five independent variables tracking

Table 1: *Mass of agglomerates (in grams) in experiments*

	ratio water/PEG4000 [wt%]					
	50/50				**70/30**	**90/10**
impeller speed [rpm]	time [s]					
	10	20	40	80	80	80
600	19.60	7.10	6.50	5.45	3.00	0.80
900	2.35	1.05	0.95	0.60	0.80	0.20
1200	1.60	0.80	0.50	0.40	0.30	0.05

Table 2: *Independent variables describing a granule*

variable	notation
original solid volume	s_{o}
reacted solid volume	s_{r}
external liquid volume	l_{e}
internal liquid volume	l_{i}
pore volume	p
number of beads	n

two kinds of solid, two kinds of liquid and the pore volume of a particle. We will follow this route, making the model extension that a particle contains a certain number of equal sized entities, which we refer to as beads. Hence, a granule will be described by six independent variables, listed in table 2. The particles are assumed to be of spherical shape. This means that dependent variables such as the particle volume v, the external and internal surface area a_{e} and a_{i} and the porosity ε can be calculated as in [2].

3.2 Transformations and their rules

Particles with a composition made of the components listed in table 2 make up a particle ensemble in the granulator. Within this equipment these particles can undergo the following transformations [2]:

1. Coalescence of particles
2. Compaction (porosity reduction)
3. Chemical reaction
4. Mass transfer of liquid into the pores (penetration)
5. Breakage

The rate laws for the aforementioned transformations will be for the most part similar to the ones in [2], but changes will be made in order to incorporate the influence of the impeller speed and the binder composition. These two parameters have been identified as playing a significant role in the granulation process.

In this section we highlight only the most significant details of the transformations. Further details can be found in appendix A.

3.2.1 Coalescence

The coalescence of two particles with properties x and x' is described by the coalescence kernel $K(x, x')$. In the current study we make use of a new kernel with the following

structure,

$$K(x, x') = n_{\text{impeller}}\, \widehat{K}_0\, \widetilde{K}(x, x') \quad , \tag{1}$$

with n_{impeller} being the rotational speed of the impeller and $\widehat{K}_0$ the collision rate constant of the particles, and the coalescence efficiency $\widetilde{K}(x, x')$ defines whether coalescence occurs or not. This is decided using the Stokes criterion, i. e. the critical Stokes number $\mathrm{St}_{\mathrm{v}}^{*}$ has to be bigger than or equal to the viscous Stokes number St_{v}, so that

$$\widetilde{K}(x, x') = \mathbb{1}_{\{\mathrm{St}_{\mathrm{v}}^{*} \geq \mathrm{St}_{\mathrm{v}}\}} \quad [1] \quad . \tag{2}$$

The rules of how to calculate the Stokes numbers and other details about the kernel such as the dependency on the impeller speed can be found in appendix A.1.

The viscous Stokes number St_{v} is dependent on the collision velocity U_{col}. This important parameter of the model framework will be computed as follows:

$$U_{\text{col}} = 2\,\pi\,\widetilde{u}_{\text{col}}\, n_{\text{impeller}}\, r_{\text{impeller}} \quad , \tag{3}$$

where $\widetilde{u}_{\text{col}}$ is the ratio of collision velocity to impeller tip speed, and r_{impeller} the impeller radius. Eq. 3 follows from the analysis of various studies in which the velocity fields in granulators have been measured using different techniques, namely positron emission particle tracking (PEPT) and particle image velocimetry (PIV). A short summary of these findings is given in appendix A.1.

3.2.2 Compaction

We adopt the approach used in [2]. Details can be found in appendix A.2.

3.2.3 Chemical reaction

Chemical reaction such as the solidification of the binder on the surface of a particle and inside the pores shall be considered as a transformation in the current model framework. We follow the approach in a previous study [2]. Further details about the transformation are given in appendix A.3. Although the rate laws are the same as in [2], the rate constants will be different in the current study as different materials are used. These constants are unknown and need to be estimated from experimental results.

3.2.4 Penetration

In contrast to coalescence and compaction, the collision velocity U_{col} does not have any effect on the migration of binder on the particle surface into the pores. Moreover, other variables will govern this process. The most significant one of them is the binder viscosity η, so that the penetration rate r_{pen} will be computed by:

$$r_{\text{pen}} = \widehat{k}_{\text{pen}}\, \eta^{-1/2}\, l_{\text{e}}\, (p - l_{\text{i}}) \quad . \tag{4}$$

[1] $\mathbb{1}_{\{\mathrm{St}_{\mathrm{v}}^{*} \geq \mathrm{St}_{\mathrm{v}}\}} = \begin{cases} 1 & \text{, if} \quad \mathrm{St}_{\mathrm{v}}^{*} \geq \mathrm{St}_{\mathrm{v}} \\ 0 & \text{, otherwise} \end{cases}$

The dependency of the penetration rate on the binder viscosity is a new feature of the granulation model. A more detailed analysis of the transformation and further aspects regarding its computation are given in appendix A.4.

3.2.5 Breakage

With respect to breakage, it should be noted that the system contains three different particle "types", all described by the same particle model. Namely we have

- droplets: $s_\mathrm{o} = 0,\ s_\mathrm{r} = 0,\ l_\mathrm{e} = v,\ l_\mathrm{i} = 0,\ p = 0$
- solid cores with external liquid and a non-breakable solid core ($v - l_\mathrm{e}$): $s_\mathrm{o} > 0,\ s_\mathrm{r} \geq 0,\ l_\mathrm{e} \geq 0,\ l_\mathrm{i} \geq 0,\ p \geq 0$
- "real" agglomerates: $s_\mathrm{o} > 0,\ s_\mathrm{r} \geq 0,\ l_\mathrm{e} \geq 0,\ l_\mathrm{i} \geq 0,\ p > 0 \quad .$

In order to describe the breakage transformation, one has to know the breakage frequency of the particles and their daughter particle distribution. The breakage frequency is a measure of the likelihood that a particle breaks. This is likely to depend on the operating conditions, so that the breakage frequency in the current model is dependent on the impeller speed. We assume that the breakage has binary character, so that the transformation results in an abraded parent particle and a daughter particle. In contrast to [2], the daughter particle distribution does not only depend on the size of the parent particle but also on its composition.

Breakage frequency In the literature, e. g. [30], it is reported that the breakage probability, for instance in milling, is proportional to the applied kinetic energy, i. e. to the square of the impact velocity U_imp. As the energy is introduced into the system by the impeller movement, we anticipate that particle breakage is caused by impeller-particle collisions. The impact velocity U_imp is the speed differential between the tip speed and the particle velocity. Hence we get,

$$U_\mathrm{imp} = 2\,\pi\,\widetilde{u}_\mathrm{imp}\,n_\mathrm{impeller}\,r_\mathrm{impeller} \tag{5}$$

$$= 2\,\pi\,(1 - \widetilde{u}_\mathrm{col})\,n_\mathrm{impeller}\,r_\mathrm{impeller} \quad . \tag{6}$$

Due to the solidification of the binder the particles are expected to gain strength, i. e. will be less likely to break. Therefore a function $\Psi(s_\mathrm{r})$ is introduced,

$$\Psi(s_\mathrm{r}) = 1 - \min\left(\frac{s_\mathrm{r}/\left(s_\mathrm{o} + s_\mathrm{r} + p\right)}{s_\mathrm{r}^*}, 1\right) \quad , \tag{7}$$

$$\text{with} \quad s_\mathrm{r}^* = \text{dimensionless critical amount of reacted solid so that the particle core does not break} \quad .$$

Taking these considerations into account, the breakage frequency $g(x)$ takes the following form:

$$g(x) = \begin{cases} \widehat{k}_{\text{att}}\, U_{\text{imp}}^2\ (\varepsilon\, \Psi(s_{\text{r}}) + \chi)\ v & \text{, if} \quad \begin{array}{l} \varepsilon\, \Psi = 0 \text{ and } l_{\text{e}} \geq l_{\text{e,parent,min}} \\ \varepsilon\, \Psi > 0 \text{ and } n \geq n_{\text{parent,min}} \end{array} \\ 0 & \text{, otherwise} \end{cases} \quad , \tag{8}$$

$$\text{with} \quad \varepsilon = \frac{p}{v} \ , \quad \chi = \frac{l_{\text{e}}}{v} \quad .$$

Further remarks and discussion about the breakage frequency can be found in appendix A.5.

Daughter distributions and particle composition The daughter distributions of the different types of particles have to be distinguished. This leads to following cases and conditions.

- **Case I: Droplets and particles with non-breakable solid core**

$$\varepsilon\, \Psi\,(s_{\text{r}}) = 0 \tag{9}$$

- **Case II: "Real" agglomerates**

$$\varepsilon\, \Psi\,(s_{\text{r}}) > 0 \tag{10}$$

With respect to the daughter distributions and their composition we follow the ideas from [2]. The details are given in appendix A.5.

3.3 Initial conditions for the simulations

At the start of the process two types of particles are present in the system, 350 g of nonpareils and 8 ml of binder droplets. The sugar particles are nonporous. Further it is assumed that it is sufficient to represent the particles as a monodisperse ensemble, because the material used in the experiments exhibited a narrow size range. Hence the solid particles have the following composition at the start of the process:

$$s_{\text{o}} = 4.077 \cdot 10^{-10}\,\text{m}^3, \quad s_{\text{r}} = 0\,\text{m}^3, \quad l_{\text{e}} = 0\,\text{m}^3, \quad l_{\text{i}} = 0\,\text{m}^3, \quad p = 0\,\text{m}^3 \quad .$$

Amongst the solid particles are binder droplets which have approximately a diameter of 2 mm. Therefore their composition will be,

$$s_{\text{o}} = 0\,\text{m}^3, \quad s_{\text{r}} = 0\,\text{m}^3, \quad l_{\text{e}} = 4.188 \cdot 10^{-9}\,\text{m}^3, \quad l_{\text{i}} = 0\,\text{m}^3, \quad p = 0\,\text{m}^3 \quad .$$

4 Response surface methodology

The testing and validation of the model outlined in the previous section is done through the application of an experimental design/response surface approach and optimisation.

4.1 Experimental design

When one wants to optimise the outcome of a process, reaction, etc., one can vary the parameters under scrutiny. However, varying one parameter at the time can be misleading, as combined changes of the parameters can be important and should therefore be considered as well. They often give a significant contribution towards the decision on how to proceed in the optimisation procedure. As each set of parameters represents a different experiment, one wants to keep the number of experiments as low as possible in order to achieve an optimal value within the desired, quality dictated boundaries.

These parameters z are often called factors. For each of these factors the user has to define levels, at least two. In order to get a full mapping of k factors with 2 levels each, 2^k experiments are necessary. This set of experiments allows for the calculation of the effects of each factor, which are effectively sensitivities with respect to the k parameters. For easier handling of the data it is common to code the respective variables/parameters. Therefore the parameter range is normalised to $[-1\ \ 1]$ corresponding to the lowest and highest value [20].

Although the naming implies it, the observations at each point of the experimental design do not necessarily have to come from experiments. This means the observations of the process can also be results from simulations, so that the effects of the respective model variables and parameters can be examined. Moreover, the observations can be used to construct a response surface $\zeta(z)$ that is an approximation of the "real" process behaviour,

$$\zeta(z) = f_{\text{sim}}(z) + \epsilon \tag{11}$$

$$\begin{aligned} \text{with} \qquad \zeta(z) &= \text{response surface} \\ f_{\text{sim}}(z) &= \text{value from simulation} \\ \epsilon &= \text{approximation error} \quad . \end{aligned}$$

Such a surface allows for the simple calculation of the process value for a given set of parameters without evaluating the complex model framework at this point. This means the process model is only evaluated at certain points. For cases that fall within this range of process conditions the process behaviour is approximated by the response surface. Hence the evaluation of the process behaviour for such points is done via the response surface, which has the attraction of being computationally cheap, whereas the evaluation of the complex model framework can be computationally expensive as is the case in the current study.

The simplest response surface is of first order and can be represented by following equation:

$$\zeta(z) = \beta_0 + \sum_{j=1}^{k} \beta_j \, z_j \tag{12}$$

$$\begin{aligned} \text{with} \qquad j &= \text{variable index} \\ k &= \text{number of variables} \\ \beta_0, \beta_j &= \text{parameters of surface} \quad . \end{aligned}$$

The number of parameters in eq. 12 is $1 + k$. Estimates for these parameters can be established by fitting eq. 12 to a set of observations.

4.2 Optimisation

If one wants to achieve an optimum with respect to a certain process outcome, it is possible to formulate the problem as a minimisation problem. Therefore an objective function $\Phi(z)$ is defined,

$$\Phi(z) = \sum_{i=1}^{N} \left[y_i(z) - \widetilde{y}_i \right]^2 \tag{13}$$

$$\begin{aligned} \text{with} \qquad i &= \text{experiment index} \quad (i = 1, \ldots, N) \\ y_i(z) &= \text{model response} \\ \widetilde{y}_i &= \text{observed values} \quad . \end{aligned}$$

The minimisation of the objective function $\Phi(z)$ yields the optimal parameter set z_{opt}. The model response $y(z)$ can originate from any source. This means, it can stem from a model or just from approximations of the solution such as a response surface.

The optimisation is subject to a number of constraints. There often exist physical limits for the parameters z, so that

$$z_{\text{constraints,low}} \leq z_{\text{opt}} \leq z_{\text{constraints,high}} \quad . \tag{14}$$

In case the model response is taken from a response surface, it has to be remembered that such surface is just an approximation of the model. Hence, it might be necessary due to physical reasons to impose constraints on the model solutions as well,

$$\zeta_{\text{constraints,low}} \leq \zeta(z_{\text{opt}}) \leq \zeta_{\text{constraints,high}} \quad . \tag{15}$$

5 Results and discussion

The experimental results (mass of agglomerates) (see table 1) show different trends with respect to mixing time, impeller speed and binder composition. Ideally all of the model parameters would be known, but in reality this is not the case, so that the unknown ones have to be estimated. This means that some of the model parameters were estimated in the current study, whereas the rate constants were obtained from an optimisation procedure that is discussed in the next section. Table 7 in the appendix lists all model parameters and their used values.

Using an optimisation routine would mean in practice that the complex granulation model has to be evaluated for every point at each optimisation step, which will be computationally expensive. A suitable way to avoid such problems is offered by the response surface methodology. In the current study, we chose to optimise four model parameters, namely the collision rate constant $\widehat{K}_0$, the consolidation rate constant k_{porred}, the breakage rate constant $\widehat{k}_{\text{att}}$, and the reaction rate constant(s) k_{reac}. These parameters have been chosen, as they are expected to have the most significant impact on the predictions of the model. An experimental design is set up for these parameters. Variables in experimental designs

Table 3: *Uncoded and coded variables*

uncoded variables				coded variables	
parameter	unit	"end"	value	z_j	value [-]
$\widehat{K}_0$	m^3	lower	$1.0 \cdot 10^{-10}$	1	-1
		upper	$2.0 \cdot 10^{-10}$		1
k_{porred}	s/m	lower	0.2	2	-1
		upper	0.4		1
$\widehat{k}_{\mathrm{att}}$	s/m^5	lower	$4.0 \cdot 10^7$	3	-1
		upper	$8.0 \cdot 10^7$		1
k_{reac}	m/s	lower	$2.0 \cdot 10^{-9}$	4	-1
		upper	$4.0 \cdot 10^{-9}$		1

are usually represented by coded variables [20], so that it is easy to compare the sensitivity of the model for different variables. In the simplest case each variable occurs at two levels (values), allowing the construction of a hypercube in the multidimensional space of variables. The number of corner points equals the number of possible combinations of the variables. This means for k variables with two levels each, we have 2^k combinations. Table 3 shows the set of variables used under analysis in the uncoded and coded version. The values of the variables in table 3 have been chosen after preliminary studies. One observation can be obtained from each point/simulation. In the current study, we chose the mass of agglomerates m_{agglo} as the observation, which is by definition:

$$m_{\mathrm{agglo}} = \sum_{\text{all granules}} m_{\mathrm{granule},\, n \geq 6} \quad . \tag{16}$$

This means that granules that contain six and more beads are considered as agglomerates. The mass of agglomerates as the process observation can then be used to construct the response surfaces.

5.1 Response surfaces

Linear response surfaces are used for the approximation of the model behaviour for each set of observations. Eq. 12 is fitted with a least squares approach to the data resulting in the values for the parameters $\beta_0 \ldots \beta_4$ given in table 4. Although the ratio of upper to lower values for all uncoded variables is 2:1, it is apparent from table 4 that the collision rate has the highest sensitivity amongst the considered variables for the examined settings. Further it can be noted, that the sensitivities decrease over time for the majority of the values.

By fixing two out of the four variables it is possible to plot the response surfaces. Figure 2 shows the six different combinations for the case with an impeller speed of 900 rpm and a binder composition with 50 % PEG4000 and 50 % water after 80 s. The unchanged, coded variables were set to zero ($z_j = 0$).

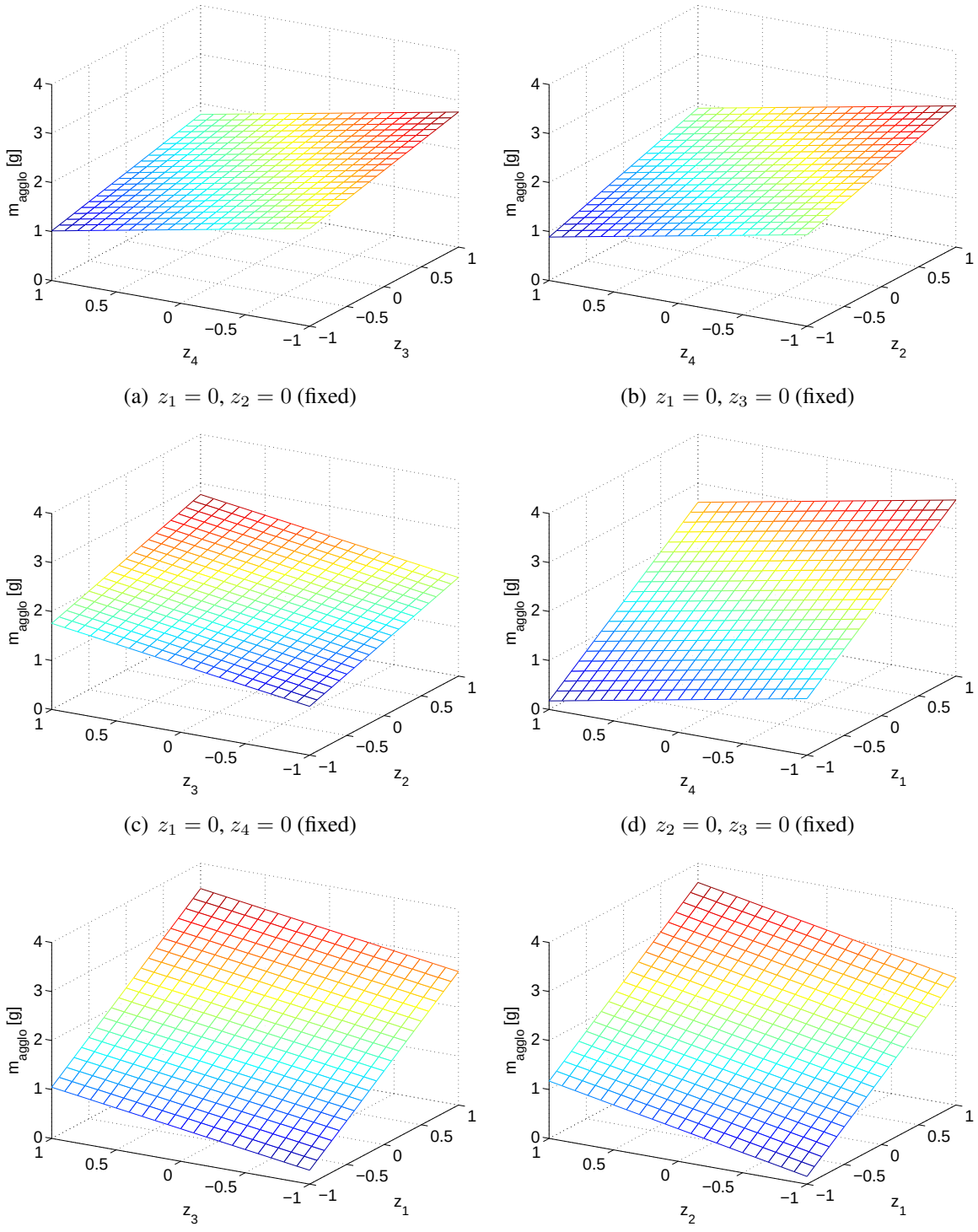

(a) $z_1 = 0$, $z_2 = 0$ (fixed)

(b) $z_1 = 0$, $z_3 = 0$ (fixed)

(c) $z_1 = 0$, $z_4 = 0$ (fixed)

(d) $z_2 = 0$, $z_3 = 0$ (fixed)

(e) $z_2 = 0$, $z_4 = 0$ (fixed)

(f) $z_3 = 0$, $z_4 = 0$ (fixed)

Figure 2: *Response surfaces with two fixed variables for 900 rpm and a water/PEG4000 ratio of 50:50 after 80 s (coefficients from table 4)*

Table 4: *Coefficients of linear response surfaces*

η [Pa s]	speed [rpm]	time [s]	β_0 [g]	β_1 [g]	β_2 [g]	β_3 [g]	β_4 [g]	residual [g]
$98 \cdot 10^{-3}$	600	10	8.5640	5.6475	1.5875	-0.9812	-0.0025	16.5915
		20	8.8394	5.3056	1.6906	-0.5106	-0.1831	13.9816
		40	7.7650	4.5813	1.5262	-0.2013	-0.5875	15.1072
		80	6.2706	3.4944	1.3294	-0.2094	-0.8394	14.4716
	900	10	5.4931	3.2394	1.4156	-0.6606	-0.0906	10.2990
		20	3.8494	2.4494	0.9819	0.4519	-0.2644	10.2223
		40	2.9400	1.8888	0.7225	0.5050	-0.3163	7.7569
		80	1.8850	1.2200	0.5075	0.3813	-0.4900	5.8167
	1200	10	2.3550	1.6138	0.6700	-0.0638	-0.0263	3.2363
		20	1.9550	1.3738	0.5463	0.0175	-0.0600	2.3370
		40	1.4613	1.0250	0.4175	-0.0538	-0.1600	1.5747
		80	0.7400	0.5338	0.2588	-0.1088	-0.1638	0.9051
$23 \cdot 10^{-3}$	600	80	0.0038	0.0038	-0.0013	-0.0000	-0.0000	0.0001
	900[2]	80	0	0	0	0	0	0
	1200[2]	80	0	0	0	0	0	0
$5 \cdot 10^{-3}$	600[2]	80	0	0	0	0	0	0
	900[2]	80	0	0	0	0	0	0
	1200[2]	80	0	0	0	0	0	0

5.2 Optimisation

With eq. 13 as the objective function the chosen model parameters are subject to optimisation. The target values $\widetilde{y}_i$ are the masses of agglomerates obtained in the experiments (cf. table 1). The model responses $y(z) = m_{\text{agglomerates}}(z)$ are not obtained from the actual granulation model, but from the response surfaces (eq. 12 and table 4). As the observations and the effects of the experimental design are actually just valid for the observed range, constraints for the variables and the model response have to be taken into account. Hence, the optimal solution z_{opt} is subject to following constraints,

$$z_{\text{constraints,low}} = (-1, -1, -1, -1) \ , \tag{17}$$

$$z_{\text{constraints,high}} = (1, 1, 1, 1) \ , \tag{18}$$

$$\zeta(z_{\text{opt}}) \geq 0 \quad . \tag{19}$$

The optimisation with the above mentioned objective function, constraints and inputs was performed with the Matlab routine `fmincon`. The optimisation consisted of four iterative steps during which the objective function was called 31 times. It took less than a second to run the optimisation on a desktop PC (Intel Pentium 4, 2.4 GHz). The optimal solution is:

$$z_{\text{opt}} = (0.4847, -1.0000, -1.0000, 1.0000) \quad . \tag{20}$$

The coded variables can be converted back to the uncoded version (table 5).

[2]The calculated masses for these cases were zero. Hence, it is only possible to construct trivial response surfaces.

Table 5: *Solution from optimisation with response surfaces*

coded variables		uncoded variables		
z_j	value [-]	parameter	unit	value
1	0.4847	$\widehat{K}_0$	m^3	$1.742 \cdot 10^{-10}$
2	-1	k_{comp}	s/m	0.2
3	-1	$\widehat{k}_{\mathrm{att}}$	$\mathrm{s/m}^5$	$4.0 \cdot 10^{7}$
4	1	k_{reac}	m/s	$4.0 \cdot 10^{-9}$

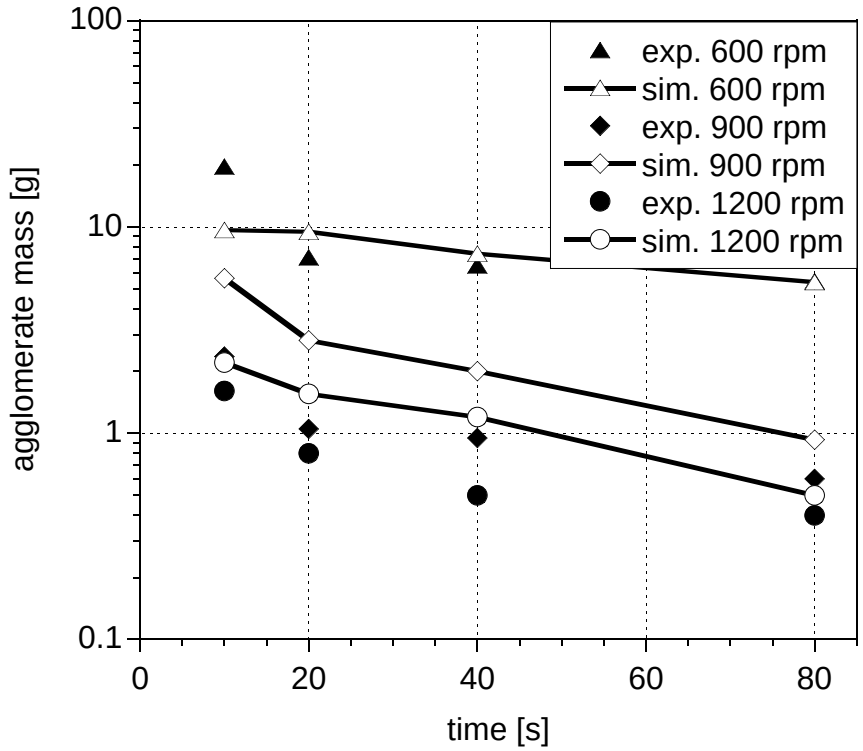

Figure 3: *Mass of agglomerates for different impeller speeds (water/PEG4000 ratio of 50:50)*

5.3 Simulation results with optimised set

Under the different process conditions the granulation model predicts different masses of agglomerates. All conditions except the impeller speed and parameters that are related to the binder composition (viscosity, density) are the same for the various cases. The values used for the various parameters are summarised in table 7 in the appendix.

Fig. 3 shows the mass of agglomerates for setups with a binder having a water to PEG4000 ratio of 50:50 and variable impeller speed at the different times. As it has been observed in the experiments, the mass of agglomerates is decreasing over time. The simulation results follow the same trend. Furthermore the same order and distances between the data with respect to the impeller speed as in the experiments are achieved, although the values for the mass of agglomerates from the simulations do not always match perfectly the ones

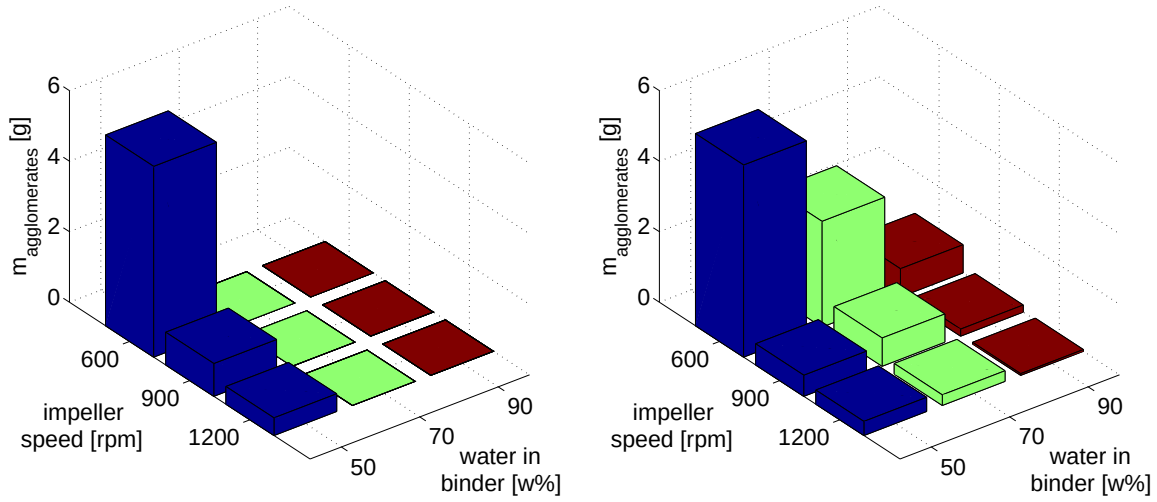

(a) Simulation results

(b) Experimental results

Figure 4: *Mass of agglomerates after 80 s for different combinations of impeller speed and binder composition*

from the experiment.

A variation in the composition of the binder, i. e. its viscosity and density, at $t = 80\,\mathrm{s}$ leads to fig. 4(a). It turns out that the model does not predict the formation of agglomerates when the fraction of water in the binder is increased from 50 to 70 or even 90 percent. In contrast to this, the experiments lead to the formation of agglomerates, although it has to be noted that the measured masses for the medium and high impeller speed are relatively small (fig. 4(b)).

With respect to product quality it is important to know the composition of the granules. Porosity is a property that is linked to the solubility or the release kinetics of an active substance. The average porosity of the particles depends on the impeller speed and on the binder composition (fig. 5). There is a clear distinction between the setups with a binder composition of 50:50 to the ones with the other two binders. For a binder with 50 w% PEG4000 the system that is produced with the highest impeller speed exhibits the lowest porosity. Apparently it does not stay constant over time but decreases towards the end of the process. A reduction of the impeller speed leads to the formation of a system that has a porosity that is approximately 5 % higher than in the former case. Although the porosity is declining over time as well, a small maximum can be observed at 20 s. Such a maximum can also be spotted for the case with the lowest impeller speed whose porosity is again increased by 5 %, although this is not the case for early times. An increase of the fraction of water in the binder results in systems with a much lower porosity. Only the setup with the lowest impeller speed (binder composition of 70:30) promotes the formation of porous particles, whereas the systems evolving from different conditions do not possess porosity.

Only particles that contain at least two beads ($n \geq 2$) can be porous. As fig. 5 shows just the porosity for the entire system, i. e. all particles, it is worthwhile to have a look at the porosity of the particles that can actually be porous. Therefore fig. 6 shows the evolution of the average porosity of particles with at least two beads for different process conditions.

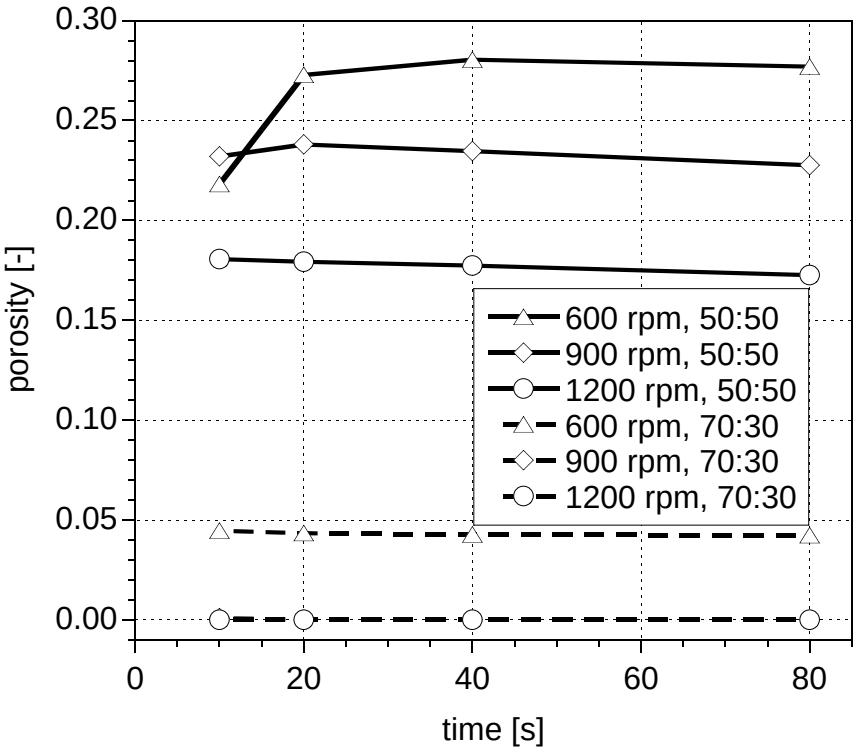

Figure 5: *Average porosity of all particles for different cases (simulation)*
[3]

Once again we can observe the clear dependency of the porosity on impeller speed, although the spread is not as big as for the overall porosity. However, for a binder composition of 50:50 the porosity is decreasing for all impeller speeds over time, in absolute terms more for the case with the lowest impeller speed, not so much for the other two cases. It is interesting to note that the particle porosity for the lowest impeller speed and a binder composition of 70:30 is at all times higher than for the 50:50 composition and the highest impeller speed. This trend is actually completely different from the overall porosity (fig. 5). Although the last case does not lead to the formation of agglomerates ($n \geq 6$), fig. 6 reveals that granules ($n \geq 2$) are formed. However, they are just not big enough to be classified as agglomerates.

As the porosity in the previous figures is just an average measure, the case with the lowest impeller speed and the 50:50 binder composition has been chosen to show the evolution of the porosity across the different particle sizes over time (fig. 7). At the beginning ($t = 10\,\mathrm{s}$) the vast majority of porous particles contains two beads and has a porosity of nearly $30\,\%$. As the time goes by we see a broadening of the distribution. This means particles with two beads "develop" a lower porosity over time. Although this porosity is below the minimum porosity when compaction/pore volume reduction would occur, the porosity is decreasing over time due to chemical reaction. In fact, the binder inside the

[3] For a binder composition of 90:10 no porous particles are present in the system, so that these cases are not displayed in the figure in order to keep it tidy.

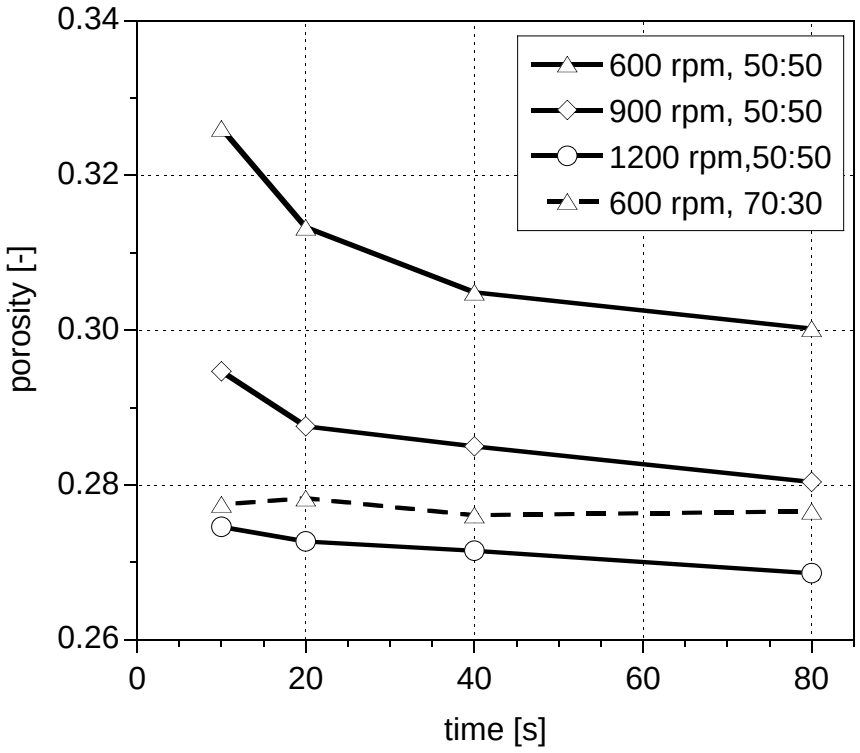

Figure 6: *Average porosity of particles with at least 2 beads for different cases (simulation)*

pores (internal liquid l_i) is solidifying and therefore reduces the pore volume. However, the rise of porous particles with three and more beads can also be noticed, whose porosity can be as high as 50 %.

An important feature of the model is the incorporation of reaction in the granule. In the present case this is the solidification of the (reactive) binder. A new component s_r is formed from external and internal liquid, l_e and l_i. In order to monitor the progress of such conversion we define a conversion ratio y_{s_r} as follows,

$$y_{s_\mathrm{r}} = \frac{\sum_{\text{all particles}} s_\mathrm{r}}{\sum_{\text{all particles}} s_\mathrm{r} + l_\mathrm{e} + l_\mathrm{i}} \quad . \tag{21}$$

Figure 8 shows the average conversion ratio of the binder over time for different conditions. The increase in the amount of reacted binder roughly follows a linear trend. The data can be divided into two groups. The first group includes the setup with binder having a PEG4000/water ratio of 50:50. Within this group there is no obvious dependency of the conversion ratio on the impeller speed. It can only be noted that the setup with the medium impeller speed yields the highest conversion ratio at all times. However, for the low and high rotational speed, the trends are changing over time. The second group of conversion ratios is made of the other two binder composition setups. In contrast to the first group, a clear dependency on the impeller speed can be observed. A higher impeller speed leads to higher conversion ratios, though lower than for the first group. Except for the lowest impeller speed of 600 rpm the trends for the setups with both binder compositions are identical.

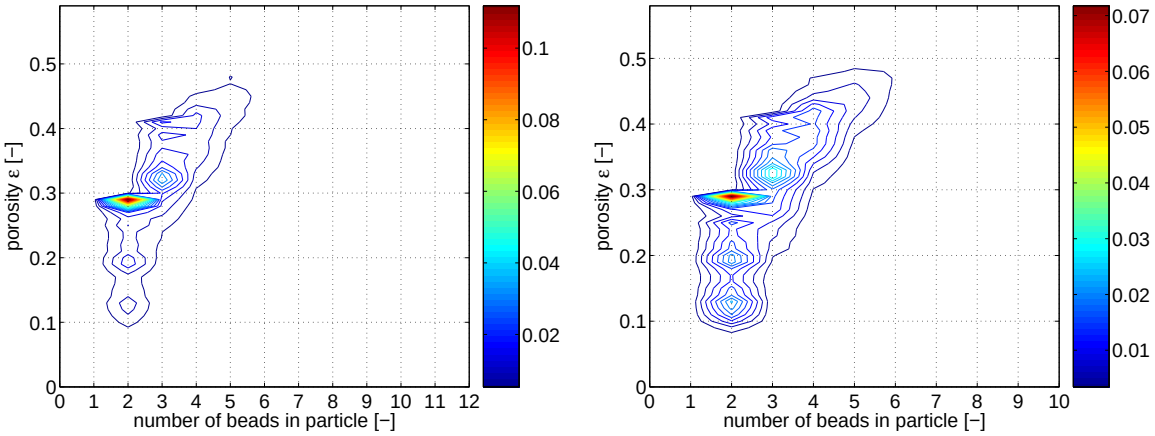

(a) After 10 s (b) After 20 s

(c) After 40 s (d) After 80 s

Figure 7: *Porosity of particles with at least 2 beads for an impeller speed of 600 rpm and 50:50 binder composition*

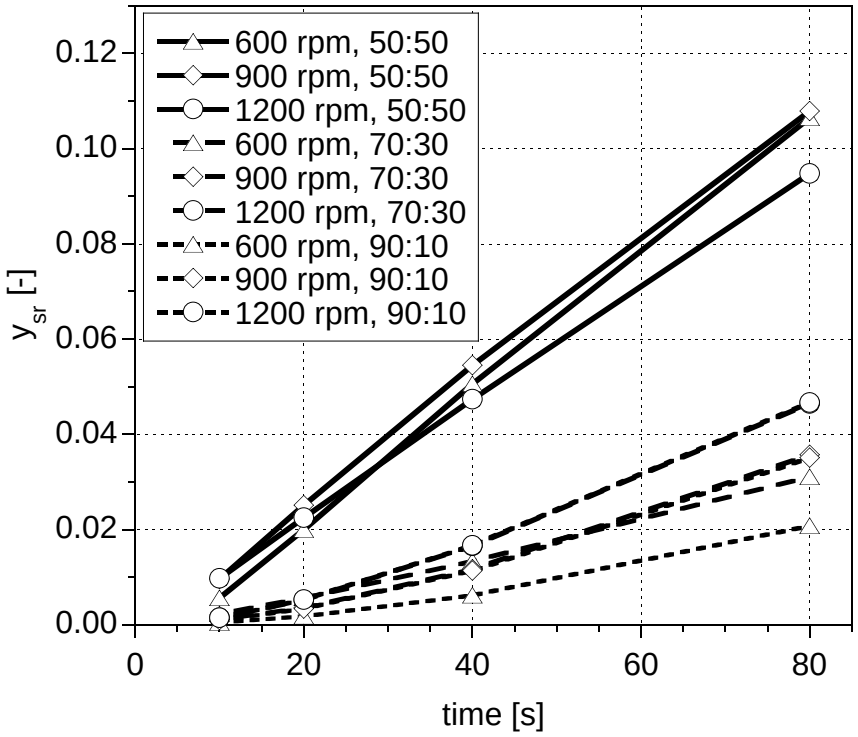

Figure 8: *Average conversion ratio of binder into reacted solid over time for all combinations of binder composition and impeller speed*

Event statistics Coalescence events take place according to the Stokes criterion. This means that a certain number of particle-particle collisions will lead to coalescence. The dependency of this ratio on the process setup and the time is plotted in figure 9. After 30 s the ratios reach steady state at the latest. The influence of the impeller speed on the ratio between coalescence events to collision events is shown in fig. 9(a). It is apparent that steady state is reached faster as the impeller speed increases. For the same impeller speed but different binder compositions the trends look slightly different (fig. 9(b)). Whereas the setup with a binder composition of 50:50 results in a monotonic increase of the coalescence to collisions ratio until it reaches steady state, a significant increase and decrease of this ratio over time can be observed for a binder composition of 70:30. Although there are not any coalescence events of two solid particles for the case with a binder composition of 90:10, i. e. with at least one bead each, the ratio of coalescence to collision events is still bigger than zero. This behaviour can be explained with the break off and coalescence of liquid droplets.

The granulation process exhibits two competing processes: coalescence and breakage. The ratios of coalescence to breakage events for different setups are plotted in fig. 10. Steady-state is once again reached after 30 seconds at the latest, earlier for the high impeller speed, later for the lowest impeller speed (fig. 10(a)). This behaviour results from the interaction of the different subprocesses of granulation as depicted in fig. 1. At the beginning the granulation is dominated by coalescence events that are being matched by the number of breakage events when steady-state is reached. Furthermore it is noticeable that the maxima in the coalescence to breakage ratio depends on the impeller speed at the

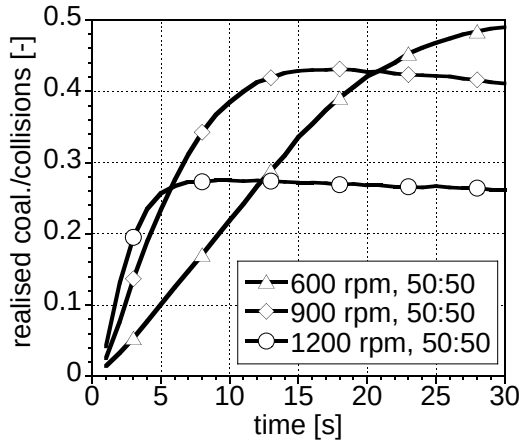

(a) Variation of the impeller speed (binder composition 50:50)

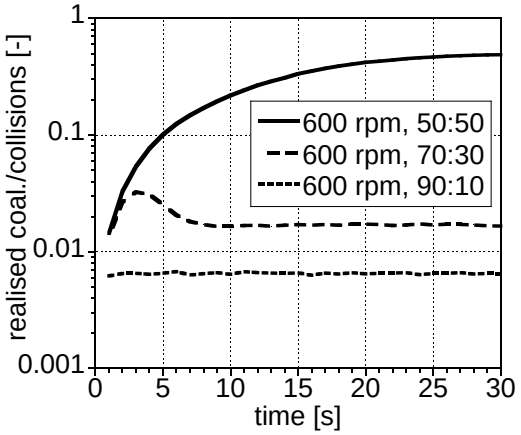

(b) Variation of binder composition (impeller speed of 600 rpm)

Figure 9: *Ratio of coalescence to collision events for* $t = 0 \ldots 30\,\mathrm{s}$

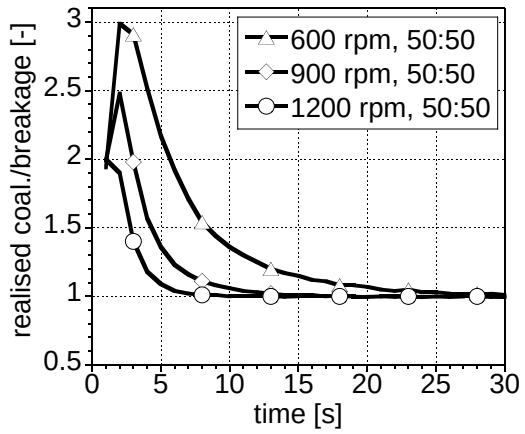

(a) Variation of the impeller speed (binder composition 50:50)

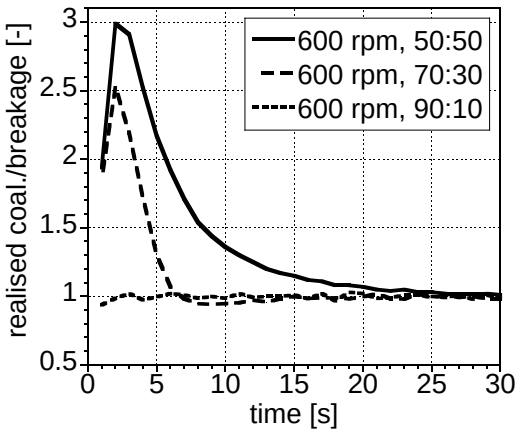

(b) Variation of binder composition (impeller speed of 600 rpm)

Figure 10: *Ratio of coalescence to breakage events for* $t = 0 \ldots 30\,\mathrm{s}$

same binder composition. Similar behaviour can be observed, when the impeller speed is fixed but the binder composition varied (fig. 10(b)).

6 Conclusions

A multidimensional model for granulation has been presented in this paper. It is based on the model outlined in [2]. The particle description has been extended, allowing the number of equal sized entities in a particle to be tracked. Hence a particle is described by six dimensions. The collision rate of the particles, being part of the coalescence kernel, is now dependent on the impeller speed. The breakage frequency of the particles is proportional to the introduced kinetic energy, which is represented by the square of the impeller speed. Furthermore we allow particles to gain strength due to the formation of reacted solid, so that their breakage becomes less likely. The dependence of the binder penetration on the dynamic viscosity as an important binder property is now reflected in the rate law. The granulation model contains quite a few parameters. Some of them can be measured, whereas others have to be estimated. However, through the use of experimental data it is possible to obtain some of the model parameters from an optimisation. A response surface approach was employed in order to allow for an easier evaluation of the model response. Four important model parameters of the subprocesses were optimised, namely the collision rate constant, the compaction rate constant, breakage rate constant, and the reaction rate constant. Simulations with the complete set of parameters for varying process conditions in the impeller speed and binder composition reveal that the simulation results follow the same trends as the experiments. This means, the mass of agglomerates is decreasing as the granulation process progresses. A reduction in the mass of agglomerates can also be observed when the impeller speed, and hence the introduced kinetic energy, is increased. As the fraction of water in the binder is increased, less granules are formed. Apparently no particles with a certain size (agglomerates) are present in any system with binder compositions of 70:30 and 90:10 at the end of the process. Although this trend matches qualitatively with the experiments in which the mass of agglomerates decreases with a higher water amount in the binder (= lower viscosity), it shows that there are still a few limitations in the model. It can be concluded that the combined use of the multidimensional granulation model, the response surface methodology and a suitable set of experimental data is a valid approach to gain more insight into granulation processes. In order to broaden the base for the comparison between model and experiments, it is conceivable in the future to incorporate additional measures so that the multidimensional model can eventually be compared with multidimensional experimental data.

Notation

a	surface area, m^2
C	constant for calculation of internal surface area from pore volume, -
d	diameter, m
e	coefficient of restitution, -
f_{att}	probability density of daughter particles, -
g	breakage frequency, s^{-1}
h	external liquid layer thickness, m
h_{a}	characteristic length scale of surface asperities, m
K	coalescence kernel, $\mathrm{m}^3\,\mathrm{s}^{-1}$
K_0	collision rate, $\mathrm{m}^3\,\mathrm{s}^{-1}$
$\widehat{K}_0$	size-independent part of coalescence kernel, m^3
$\widetilde{K}$	size-dependent part of coalescence kernel (coalescence efficiency), -
$\widehat{k}_{\mathrm{att}}$	rate constant for breakage, $\mathrm{s}\,\mathrm{m}^{-5}$
$\widehat{k}_{\mathrm{pen}}$	rate constant for penetration, $\mathrm{kg}^{1/2}\,\mathrm{s}^{-3/2}\,\mathrm{m}^{-7/2}$
k_{porred}	rate constant for consolidation, $\mathrm{s}\,\mathrm{m}^{-1}$
k_{reac}	rate constant for chemical reaction, $\mathrm{m}\,\mathrm{s}^{-1}$
l	liquid volume, m^3
m	mass, kg
$\widetilde{m}$	harmonic mean granule mass, kg
n	number of beads (in a particle), -
n_{impeller}	impeller speed, s^{-1}
p	pore volume, m^3
$\widetilde{R}$	harmonic mean particle radius, m
r	reaction rate, $\mathrm{m}^3\,\mathrm{s}^{-1}$
r_{impeller}	impeller radius, m
St_{v}	Stokes number, -
$\mathrm{St}_{\mathrm{v}}^*$	critical Stokes number, -
s	solid volume, m^3
s_{r}^*	dimensionless critical amount of reacted solid, -
t	time, s
U_{col}	collision velocity, $\mathrm{m}\,\mathrm{s}^{-1}$
U_{imp}	impact velocity, $\mathrm{m}\,\mathrm{s}^{-1}$
$\widetilde{u}_{\mathrm{col}}$	ratio of collision velocity to impeller tipspeed, -
$\widetilde{u}_{\mathrm{imp}}$	ratio of impact velocity to impeller tipspeed, -
v	particle volume, m^3
y	model response, $[y]$
$\widetilde{y}$	target value (in optimisation), $[\widetilde{y}]$
$y_{s_{\mathrm{r}}}$	conversion ratio reacted solid, -
z	set of variables in response surfaces and optimisation, $[z]$

Greek letters

α	distribution parameter for discrete breakage, -
β	distribution parameter for discrete breakage, -
β	parameter of response surface, $[\beta]$
Γ	shear rate, s^{-1}
γ	surface tension, $\mathrm{N\,m}^{-1}$
ε	porosity, -
ζ	response surface, $[\zeta]$
η	dynamic (binder) viscosity, $\mathrm{Pa\,s}$
Θ	dimensionless particle volume, -
λ	surface ratio, -
$\nu_{\max}$	constant for determination of maximum fragment size, -
$\nu_{\min,\max}$	constant for determination of minimal maximum fragment size, -
ρ	density, $\mathrm{kg\,m}^{-3}$
Φ	objective function, $[\Phi]$
χ	ratio of external liquid volume to total volume, -
Ψ	weight function of reacted solid, -

Subscripts

agglo	agglomerates
att	attrition/breakage
e	external
frag	fragment
i	internal
j	particle index
k	particle index
max	maximum
min	minimum
o	original
parent	parent particle
pen	penetration
r	reacted
reac	reaction
I	breakage case I
II	breakage case II

Acknowledgements

Andreas Braumann would like to thank Procter and Gamble, and the University of Cambridge for funding. Markus Kraft thanks the EPSRC (grant EP-E01772X) for financial

support.

A Further details of transformations

A.1 Coalescence

The coalescence efficiency $\widetilde{K}$ is calculated based on the Stokes criterion, which is a function of the viscous Stokes number and the critical Stokes number (eq. 2). The viscous Stokes number $\mathrm{St_v}$ is computed as

$$\mathrm{St_v} = \frac{\widetilde{m}\, U_{\mathrm{col}}}{3\,\pi\,\eta\,\widetilde{R}^2} \quad , \tag{22}$$

where $\widetilde{m}$ is the harmonic mean granule mass, U_{col} is the collision velocity, η is the binder viscosity, and $\widetilde{R}$ is the harmonic mean particle radius. The critical Stokes number $\mathrm{St_v^*}$ is defined by:

$$\mathrm{St_v^*} = \left(1 + \frac{1}{e_{\mathrm{coag}}}\right) \ln\left(\frac{h}{h_{\mathrm{a}}}\right) \quad , \tag{23}$$

where e_{coag} is the coefficient of restitution, h is the thickness of the binder layer, and h_{a} is the characteristic length scale of surface asperities.

The coalescence kernel $K(x, x')$ in eq. 1 contains a dependency on the impeller speed n_{impeller}. This relationship uses the findings of [5]. The authors studied different coalescence kernels and concluded that the 'induced shear kernel (ISK)' seems to be best suited for granulation processes. According to [5] the collision rate K_0 takes the form,

$$\begin{aligned} K_0 &= \frac{4}{3}\,\Gamma\,(d_j + d_k)^3 \\ &\text{with} \quad \Gamma = \text{shear rate} \\ &\qquad\; d_j, d_k = \text{diameters of particle j and k} \quad . \end{aligned} \tag{24}$$

Assuming that the shear rate Γ is proportional to the impeller speed, we have that the collision rate K_0 is proportional to the impeller speed,

$$K_0 \sim n_{\mathrm{impeller}} \quad . \tag{25}$$

Although eq. 24 states a dependency of the collision rate on the size of the particles, it is neglected in the current model framework as we expect particles of similar size.

Several studies report on the measurement of velocity fields in granulators. Two techniques have been used in these studies—positron emission particle tracking (PEPT) and particle image velocimetry (PIV).

The PEPT technique uses radioactive tracer particles and is hence capable of tracking the particle flow within a powder. It has been shown that for the mixing of wet particles in a

granulator with a vertical impeller axis, the angular speed of the particles is approximately a tenth of the impeller speed [18].

In contrast to PEPT, the PIV technique can only provide the particle velocities on the surface of a powder bed. For instance, a glass bead-water system was studied [21]. They found that the circumferential particle velocity takes values between 1.3 m/s (dimensionless radius = 0.7) and 0.5 m/s (dimensionless radius = 1.0) with the impeller tip speed being 5.65 m/s. The behaviour is similar for different fractions of water, although the actual velocity values differ slightly depending on the water fraction.
In a different study experiments with calcium carbonate and two different binders (PEG-400 ($\eta = 93\,\mathrm{mPa\,s}$) and glycerol ($\eta = 890\,\mathrm{mPa\,s}$)) were performed [22]. A dependency of the average bed velocity on the binder viscosity was found. The bed velocity was 1.21 m/s for PEG-400, whereas particles moved with 0.75 m/s when glycerol was used. The impeller tip speed was with 4.66 m/s the same one for both setups.
Recent findings [3] suggest that the tangential particle velocity in a high shear mixer "is one order of magnitude less than the impeller tip speed".

A.2 Compaction

Each particle collision leads to compaction. The porosity change $\Delta\varepsilon$ due to collision is described by:

$$\Delta\varepsilon = \begin{cases} k_{\mathrm{porred}}\, U_{\mathrm{col}}\, (\varepsilon - \varepsilon_{\mathrm{min}}) & \text{, if} \quad \varepsilon - \Delta\varepsilon \geq \varepsilon_{\mathrm{min}} \\ 0 & \text{, otherwise} \quad , \end{cases} \tag{26}$$

where k_{porred} is the rate constant of porosity reduction, U_{col} is the collision velocity, and $\varepsilon_{\mathrm{min}}$ is the minimum porosity.

A.3 Chemical reaction

The rates r_{reac} for the chemical reaction take the following forms:

Reaction on the external surface:

$$r_{\mathrm{reac,e}} = \begin{cases} k_{\mathrm{reac,e}}\, a_{\mathrm{e}}\, \dfrac{l_{\mathrm{e}}}{l_{\mathrm{e}} + s_{\mathrm{r}}} & \text{, if} \quad s_o > 0 \text{ and } l_{\mathrm{e}} > 0 \\ 0 & \text{, otherwise} \quad . \end{cases} \tag{27}$$

Reaction on the internal surface:

$$r_{\mathrm{reac,i}} = \begin{cases} k_{\mathrm{reac,i}}\, a_{\mathrm{i}}\, \dfrac{l_{\mathrm{i}}}{l_{\mathrm{i}} + s_{\mathrm{r}}} & \text{, if} \quad s_o > 0 \text{ and } l_{\mathrm{i}} > 0 \\ 0 & \text{, otherwise} \quad . \end{cases} \tag{28}$$

With the assumption that all liquids and the solidified binder have the same density ($\rho_{\mathrm{l_e}} = \rho_{\mathrm{l_i}} = \rho_{\mathrm{s_r}}$), the changes of the granule components are given by:

$$\frac{\mathrm{d}s_{\mathrm{o}}}{\mathrm{d}t} = 0, \qquad \frac{\mathrm{d}s_{\mathrm{r}}}{\mathrm{d}t} = r_{\mathrm{reac,e}} + r_{\mathrm{reac,i}}, \tag{29}$$

$$\frac{\mathrm{d}l_{\mathrm{e}}}{\mathrm{d}t} = -r_{\mathrm{reac,e}}, \qquad \frac{\mathrm{d}p}{\mathrm{d}t} = \frac{\mathrm{d}l_{\mathrm{i}}}{\mathrm{d}t} = -r_{\mathrm{reac,i}} \quad . \tag{30}$$

A.4 Penetration

Consider a droplet sitting on the surface of a powder bed [10]. The volume change of the droplet $\mathrm{d}l/\mathrm{d}t$ due to penetration into N_{c} pores with radius R_{pore} is given by

$$\frac{\mathrm{d}l}{\mathrm{d}t} = N_{\mathrm{c}}\, R_{\mathrm{pore}}^2 \left(\frac{R_{\mathrm{pore}}\, \gamma_{\mathrm{LV}}\, \cos\Theta_{\mathrm{d}}}{8\,\eta\, t} \right)^{1/2} \quad . \tag{31}$$

The volume change of the droplet $\mathrm{d}l/\mathrm{d}t$ is nothing more than the penetration rate r_{pen}. The comparison of eq. 31 and the expression for r_{pen} stated in [2] reveals their connection.

$$\underbrace{\frac{\mathrm{d}l}{\mathrm{d}t}}_{r_{\mathrm{pen}}} = \underbrace{\frac{\pi}{2\sqrt{2}}\, \eta^{-1/2} \left(\frac{\gamma_{\mathrm{LV}}\, \cos\Theta_{\mathrm{d}}}{t} \right)^{1/2}}_{k_{\mathrm{pen}} \;\cdot\; l_{\mathrm{e}}} \underbrace{\frac{N_{\mathrm{c}}\, R_{\mathrm{pore}}^{5/2}}{(p - l_{\mathrm{i}})}}_{} \quad . \tag{32}$$

Hence, in the current study, the penetration rate r_{pen} will be equated as follows:

$$r_{\mathrm{pen}} = \widehat{k}_{\mathrm{pen}}\, \eta^{-1/2}\, l_{\mathrm{e}}\, (p - l_{\mathrm{i}}) \quad . \tag{4}$$

This means the penetration rate is dependent upon the binder viscosity. However, the dependency on the surface tension γ_{LV} and the contact angle Θ_{d} as it is suggested in eq. 32 will be neglected. As a polyethyleneglycol based binder is used in the experiments that are used for the comparison with the current model, it is worthwhile looking at the dependency of the surface tension and viscosity on the PEG concentration. A recent study [4] investigated the influence of the PEG concentration in an aqueous PEG400 solution on the surface tension. Together with the viscosity data for PEG1000 solutions [8] ($T = 298\,\mathrm{K}$) the ratio between the surface tension and the viscosity can be calculated for varying compositions of the solutions assuming that the trend for the viscosity of PEG400 and PEG1000 solutions is quite similar. The results are presented in table 6. The data in table 6 show a clear trend. With an increasing mass fraction of PEG in the solution, the term $(\gamma/\eta)^{1/2}$, i. e. the penetration rate, decreases. The trend is mainly dominated by the varying viscosity. The changes of the components of a granule due to the penetration of binder equate to

$$\frac{\mathrm{d}s_{\mathrm{o}}}{\mathrm{d}t} = 0, \quad \frac{\mathrm{d}s_{\mathrm{r}}}{\mathrm{d}t} = 0, \tag{33}$$

$$\frac{\mathrm{d}l_{\mathrm{e}}}{\mathrm{d}t} = -r_{\mathrm{pen}}, \qquad \frac{\mathrm{d}l_{\mathrm{i}}}{\mathrm{d}t} = r_{\mathrm{pen}}, \qquad \frac{\mathrm{d}p}{\mathrm{d}t} = 0 \quad . \tag{34}$$

Table 6: *Ratio of surface tension to viscosity for aqueous PEG solutions*

w_{PEG} [wt%]	γ_{PEG400} $[\mathrm{mN\,m^{-1}}]$	η_{PEG1000} $[\mathrm{mPa\,s}]$	$(\gamma/\eta)^{1/2}$ $\left[(\mathrm{m/s})^{1/2}\right]$
0.50	35	24.3	1.2
0.30	45	9.2	2.2
0.10	50	5.2	3.1

A.5 Breakage

Breakage frequency

Amongst other variables the breakage frequency $g(x)$ (eq. 8) is dependent on the particle porosity ε. The effect that the porosity ε has on the strength of the particles is still under debate. According to [16] granules are weaker if they have a higher porosity. In addition to this, [19] found that particles with higher saturated pores are more difficult to break (porosity was constant for different saturation levels). This suggests that the breakage frequency is more likely to be proportional to the empty pore volume $(p - l_{\mathrm{i}})$. However, other sources claim that an increasing pore saturation can also lead to a reduced particle strength. As there is still disagreement about the influence, we keep our model simple, using the outlined dependency of the breakage frequency on the porosity.
Although we do not make use of it, it is worthwhile mentioning that the granule strength decreases with decreasing surface tension of the binder [16].

The breakage frequency $g(x)$ depends also on the binder viscosity according to [19, 29], i. e. the breakage frequency decreases with increasing viscosity. Given the fact that the binder viscosity in the current case is lower than in most cases in [19, 29] and that the primary particle size is much bigger, we can assume that all particles will break independently of the binder viscosity.

Although we are not using it in our model framework, we want to mention that other concepts exist in order to decide whether particles will break. For instance one can define the Stokes number due to deformation. This characteristic relates the kinetic energy the particle is exposed to to the granule strength [27]. When the Stokes number is bigger than a critical Stokes number, the particles will break. However, the strength of the particles is related to their composition. Hence, this approach takes just another view on the breakage likelihood of the particles, so that the approach using the breakage frequency is absolutely valid.

Daughter distributions and particle composition

Droplets and particles with non-breakable solid core (case I) These particles are characterised by the condition

$$\varepsilon\,\Psi\left(s_{\mathrm{r}}\right) = 0 \quad . \tag{9}$$

The size distribution of the daughter particles is modelled by a beta distribution whose probability density is given by

$$f_{\mathrm{att}}(\Theta) = \frac{1}{B(a,b)}\,\Theta^{a-1}\,(1-\Theta)^{b-1} \quad \text{with} \quad B(a,b) = \int_0^1 \Theta^{a-1}\,(1-\Theta)^{b-1}\,\mathrm{d}\Theta \tag{35}$$

with

$$\Theta = \frac{v_{\mathrm{frag}} - v_{\mathrm{frag,min}}}{v_{\mathrm{frag,max}} - v_{\mathrm{frag,min}}} \quad , \tag{36}$$

where v_{frag} denotes the total volume of the new fragment (daughter particle). This new particle will have a minimum size $v_{\mathrm{frag,min}}$ which is assumed to be a constant value for all parent particles. In contrast to this, the maximum fragment size $v_{\mathrm{frag,max}}$ will depend on the parent particle size/amount of external liquid in the parent particle according to

$$v_{\mathrm{frag,max}} = \nu_{\mathrm{max}}\, l_{\mathrm{e,parent}} \qquad (\nu_{\mathrm{max}} \leq 0.5) \quad . \tag{37}$$

The composition of a daughter particle will be

$$s_{\mathrm{o,frag}} = 0, \quad s_{\mathrm{r,frag}} = 0, \quad l_{\mathrm{e,frag}} = v_{\mathrm{frag}}, \quad l_{\mathrm{i,frag}} = 0, \quad p_{\mathrm{frag}} = 0 \quad . \tag{38}$$

Hence, the abraded parent particle will consist of

$$\begin{aligned} s_{\mathrm{o,parent,new}} = s_{\mathrm{o,parent,old}}, \quad s_{\mathrm{r,parent,new}} = s_{\mathrm{r,parent,old}}, \quad l_{\mathrm{i,parent,new}} = l_{\mathrm{i,parent,old}}, \\ l_{\mathrm{e,parent,new}} = l_{\mathrm{e,parent,old}} - v_{\mathrm{frag}}, \quad p_{\mathrm{parent,new}} = p_{\mathrm{parent,old}} \quad . \end{aligned} \tag{39}$$

The minimum amount of external liquid in a breakable parent particle is given by

$$l_{\mathrm{e,parent,min}} = \frac{\nu_{\mathrm{min,max}}}{\nu_{\mathrm{max,I}}}\, v_{\mathrm{frag,min}} \quad . \tag{40}$$

"Real" agglomerates (case II) The breakage for this kind of particles ($\varepsilon\,\Psi > 0$) has discrete character. This means a particle with n_{parent} beads will break beadwise with the maximum of beads in the daughter particle $n_{\mathrm{frag,max}}$ given by

$$n_{\mathrm{frag,max}} = \lfloor \nu_{\mathrm{max,II}}\, n_{\mathrm{parent}} \rfloor \quad [4] \qquad (\nu_{\mathrm{max,II}} \leq 0.5) \quad . \tag{41}$$

Due to the discrete character of the breakage, a minimum parent particle size, i. e. with a minimum number of beads, will exist in this case as well as assuming that the smallest daughter particle contains one bead,

$$n_{\mathrm{parent,min}} = \left\lceil \frac{1}{\nu_{\mathrm{max,II}}} \right\rceil \quad [5] \quad . \tag{42}$$

[4] $\lfloor x \rfloor = \max\{n \in \mathbb{N} : n \leq x\}$
[5] $\lceil x \rceil = \min\{n \in \mathbb{N} : n \geq x\}$

As there is not much knowledge about the probability density function of the daughter particles sizes, we apply a simple model for the probability density function $f_{\mathrm{att,II}}(n_{\mathrm{frag}})$ which gives the likelihood of daughter particles with n_{frag} beads to occur,

$$f_{\mathrm{att,II}}(n_{\mathrm{frag}}) = \frac{\alpha\, n_{\mathrm{frag}} + \beta}{n_{\mathrm{frag,max}} \left(\dfrac{n_{\mathrm{frag,max}} + 1}{2}\, \alpha + \beta \right)} \qquad (n_{\mathrm{frag}} \in [1, n_{\mathrm{frag,max}}]) \quad . \tag{43}$$

The parameters α and β define the "shape" of the density function. For $\alpha = 0$ we get a uniform distribution. Furthermore the values for the parameters must satisfy the following condition:

$$\alpha < 0: \qquad \alpha > -\frac{\beta}{n_{\mathrm{frag,max}}} \quad (\beta > 0) \tag{44}$$

$$\alpha = 0: \qquad \beta \in \mathbb{R} \backslash \{0\} \tag{45}$$

$$\alpha > 0: \qquad \alpha > -\beta \quad \text{if } \beta \leq 0 \quad . \tag{46}$$

As the particles break beadwise, attention has to be paid to the composition of the daughter particle and the remaining parent particle. Due to the breakage event parts of the internal liquid in the pores (between the beads) will be at the external surface of the particles after the breakage event. This means, the pore volume and the amount of internal liquid will be reduced, whereas the amount of external liquid will be increased. The amount of removed pore volume and "converted" liquid is assumed to depend on the surface area of the daughter particle/fragment and the surface area of its contained beads. Hence the ratio λ will be computed by

$$\lambda = \frac{\text{surface area of daughter particle without } l_{\mathrm{e}}}{\left(\sum \text{surface area beads + pores}\right)_{\text{frag}}} \tag{47}$$

$$= \frac{\pi^{1/3} \left[6\, \dfrac{n_{\mathrm{frag}}}{n_{\mathrm{parent}}}\, \left(s_{\mathrm{o}} + s_{\mathrm{r}} + p\right)_{\text{parent}} \right]^{2/3}}{n_{\mathrm{frag}}\, \pi^{1/3} \left[\dfrac{6}{n_{\mathrm{parent}}}\, \left(s_{\mathrm{o}} + s_{\mathrm{r}} + p\right)_{\text{parent}} \right]^{2/3}} \tag{48}$$

$$= n_{\mathrm{frag}}^{-1/3} \quad , \tag{49}$$

where λ denotes the proportion of pore volume and internal liquid to be removed or converted respectively. We assign $1/n_{\mathrm{parent}}$ of each component to every bead, so that the fragment will have following composition:

$$s_{\mathrm{o,frag}} = \frac{n_{\mathrm{frag}}}{n_{\mathrm{parent}}}\, s_{\mathrm{o,parent}}, \quad s_{\mathrm{r,frag}} = \frac{n_{\mathrm{frag}}}{n_{\mathrm{parent}}}\, s_{\mathrm{r,parent}} \quad . \tag{50}$$

Although proportional to the number of beads, the pore volume will be reduced.

$$p_{\mathrm{frag}} = \left(\frac{n_{\mathrm{frag}}}{n_{\mathrm{parent}}}\, p_{\mathrm{parent}} - \lambda\, \frac{n_{\mathrm{frag}}}{n_{\mathrm{parent}}} p_{\mathrm{parent}} \right) = \frac{n_{\mathrm{frag}}}{n_{\mathrm{parent}}} p_{\mathrm{parent}} \left(1 - n_{\mathrm{frag}}^{-1/3} \right) \quad . \tag{51}$$

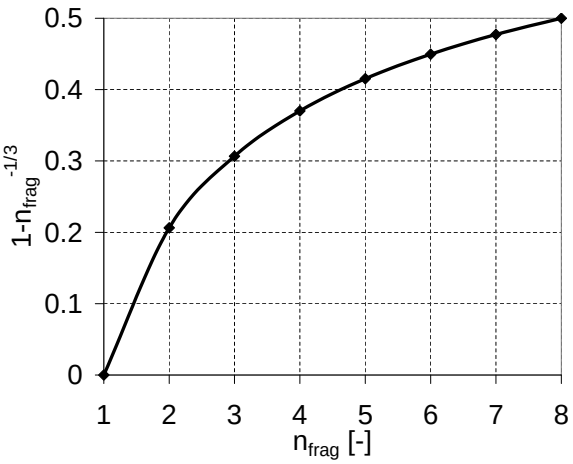

Figure 11: *Relative amount of pore volume remaining in a fragment after breakage*

By analogy the amount of internal liquid is obtained,

$$l_{\mathrm{i,frag}} = \frac{n_{\mathrm{frag}}}{n_{\mathrm{parent}}}\, l_{\mathrm{i,parent}} \left(1 - n_{\mathrm{frag}}^{-1/3}\right) \tag{52}$$

$$l_{\mathrm{e,frag}} = \frac{n_{\mathrm{frag}}}{n_{\mathrm{parent}}} \left(l_{\mathrm{e,parent}} + n_{\mathrm{frag}}^{-1/3}\, l_{\mathrm{i,parent}}\right) \quad . \tag{53}$$

In order to illustrate the proportion of pore volume that remains within a fragment the functional $(1 - n_{\mathrm{frag}}^{-1/3})$ is plotted in figure 11. The plot shows that a fragment containing just one bead will not have any pores. For fragments with two beads the pore volume will be reduced by 80 %, and for a fragment with 8 beads the pore volume is still reduced down to 50 %.

As the remaining parent particle has a breakage interface with the daughter particle, it is reasonable to assume pore volume reduction and liquid transformation for this particle as well. The composition of the abraded parent particle is computed by the following rules:

$$s_{\mathrm{o,parent,new}} = \frac{n_{\mathrm{parent}} - n_{\mathrm{frag}}}{n_{\mathrm{parent}}}\, s_{\mathrm{o,parent,old}} \tag{54}$$

$$s_{\mathrm{r,parent,new}} = \frac{n_{\mathrm{parent}} - n_{\mathrm{frag}}}{n_{\mathrm{parent}}}\, s_{\mathrm{r,parent,old}} \tag{55}$$

$$p_{\mathrm{parent,new}} = \left(\frac{n_{\mathrm{parent}} - n_{\mathrm{frag}}}{n_{\mathrm{parent}}} - \frac{n_{\mathrm{frag}}}{n_{\mathrm{parent}}}\,\lambda\right) p_{\mathrm{parent,old}} \tag{56}$$

$$= \frac{n_{\mathrm{parent}} - n_{\mathrm{frag}} \left(1 + n_{\mathrm{frag}}^{-1/3}\right)}{n_{\mathrm{parent}}}\, p_{\mathrm{parent,old}} \tag{57}$$

$$l_{\mathrm{i,parent,new}} = \frac{n_{\mathrm{parent}} - n_{\mathrm{frag}} \left(1 + n_{\mathrm{frag}}^{-1/3}\right)}{n_{\mathrm{parent}}}\, l_{\mathrm{i,parent,old}} \tag{58}$$

$$l_{\mathrm{e,parent,new}} = \frac{n_{\mathrm{parent}} - n_{\mathrm{frag}}}{n_{\mathrm{parent}}}\, l_{\mathrm{e,parent,old}} + \frac{n_{\mathrm{frag}}^{2/3}}{n_{\mathrm{parent}}}\, l_{\mathrm{i,parent,old}} \quad . \tag{59}$$

B List of used model parameters

The following table summarises the values of the model parameters used for the simulation.

Table 7: *Values of model parameters by materials and transformations*

	parameter	unit	value	origin/comment
Starting material				
solid particles	s_{o}	m^3	$4.077 \cdot 10^{-10}$	measurement [24]
	$\rho_{\mathrm{s_o}}$	$\mathrm{kg/m}^3$	1200	measurement [24]
liquid droplets	$V_{\mathrm{droplet}} = l_{\mathrm{e}}$	m^3	$4.188 \cdot 10^{-9}$	2 mm in diameter
	η_{l}	Pa s	$98/23/5 \cdot 10^{-3}$	measurement [24]
	$\rho_{\mathrm{l_e}}$	$\mathrm{kg/m}^3$	1078/1046/1012	[24]
Mixer-granulator operating parameters				
	n_{impeller}	s^{-1}	10/15/20	
	r_{impeller}	m	0.076	
	$\widetilde{u}_{\mathrm{col}}$	-	0.1	
	$\widetilde{u}_{\mathrm{imp}}$	-	0.9	$= 1 - \widetilde{u}_{\mathrm{col}}$
Breakage				
	$\widehat{k}_{\mathrm{att}}$	$\mathrm{s\,m}^{-5}$	$4.0 \cdot 10^7$	from optimisation
	s_{r}^*	-	0.05	estimate
	a	-	10	estimate
	b	-	2	estimate
	$v_{\mathrm{frag,min}}$	m^3	$9.05 \cdot 10^{-13}$	estimate
	$\nu_{\mathrm{max,I}}$	-	0.1	estimate
	$\nu_{\mathrm{min,max}}$	-	1.1	estimate
	α	-	-1	estimate
	β	-	20	estimate
	$\nu_{\mathrm{max,II}}$	-	0.5	estimate
Chemical Reaction				
	C	-	15	estimate
	$k_{\mathrm{reac,e}}$	m/s	$4.0 \cdot 10^{-9}$	from optimisation
	$k_{\mathrm{reac,i}}$	m/s	$4.0 \cdot 10^{-9}$	from optimisation
Coalescence				
	$e_{\mathrm{s_o}}$	-	1	estimate
	$e_{\mathrm{s_r}}$	-	1	estimate
	h_{a}	m	$1.0 \cdot 10^{-6}$	estimate
	$\widehat{K}_0$	m^3	$1.742 \cdot 10^{-10}$	from optimisation
Compaction				
	k_{porred}	s/m	0.2	from optimisation
	$\varepsilon_{\mathrm{min}}$	-	0.25	estimate
Penetration				
	$\widehat{k}_{\mathrm{pen}}$	$\mathrm{kg}^{1/2}\,\mathrm{s}^{-3/2}\,\mathrm{m}^{-7/2}$	$1.0 \cdot 10^{10}$	estimate

References

[1] K. Ax, H. Feise, R. Sochon, M. Hounslow, and A. Salman. Influence of liquid binder dispersion on agglomeration in an intensive mixer. *Powder Technology*, 179: 190–194, 2008. doi:10.1016/j.powtec.2007.06.010.

[2] A. Braumann, M. J. Goodson, M. Kraft, and P. R. Mort. Modelling and validation of granulation with heterogeneous binder dispersion and chemical reaction. *Chemical Engineering Science*, 62:4717–4728, 2007. doi:10.1016/j.ces.2007.05.028.

[3] A. Darelius, E. Lennartsson, A. Rasmuson, I. N. Björn, and S. Folestad. Measurement of the velocity field and frictional properties of wet masses in a high shear mixer. *Chemical Engineering Science*, 62:2366–2374, 2007. doi:10.1016/j.ces.2007.01.033.

[4] N. Derkaoui, S. Said, Y. Grohens, R. Olier, and M. Privat. PEG400 novel phase description in water. *Journal of Colloid and Interface Science*, 305:330–338, 2007. doi:10.1016/j.jcis.2006.10.008.

[5] J. A. Gantt, I. T. Cameron, J. D. Litster, and E. P. Gatzke. Determination of coalescence kernels for high-shear granulation using DEM simulations. *Powder Technology*, 170:53–63, 2006. doi:10.1016/j.powtec.2006.08.002.

[6] E. P. Gatzke and F. J. Doyle. Model predictive control of a granulation system using soft constraints and prioritized control objectives. *Powder Technology*, 121: 149–158, 2001. doi:10.1016/S0032-5910(01)00334-5.

[7] A. Gerstlauer, C. Gahn, H. Zhou, M. Rauls, and M. Schreiber. Application of population balances in the chemcial industry—current status and future needs. *Chemical Engineering Science*, 61:205–217, 2006.

[8] P. González-Tello, F. Camacho, and G. Blázquez. Density and viscosity of concentrated aqueous solutions of polyethylene glycol. *J. Chem. Eng. Data*, 39:611–614, 1994. doi:10.1021/je00015a050.

[9] M. Goodson and M. Kraft. Simulation of coalescence and breakage: an assessment of two stochastic methods suitable for simulating liquid-liquid extraction. *Chemical Engineering Science*, 59:3865–3881, 2004. doi:10.1016/j.ces.2004.05.029.

[10] K. P. Hapgood. *Nucleation and binder dispersion in wet granulation*. PhD thesis, University of Queensland, 2000.

[11] K. P. Hapgood, J. D. Litster, and R. Smith. Nucleation regime map for liquid bound granules. *AIChE Journal*, 49:350–361, 2003. doi:10.1002/aic.690490207.

[12] S. M. Iveson. Limitations of one-dimensional population balance models of wet granulation processes. *Powder Technology*, 124:219–229, 2002. doi:10.1016/S0032-5910(02)00026-8.

[13] S. M. Iveson and J. D. Litster. Growth regime map for liquid-bound granules. *AIChE Journal*, 44:1510–1518, 1998. doi:10.1002/aic.690440705.

[14] S. M. Iveson, J. D. Litster, K. Hapgood, and B. J. Ennis. Nucleation, growth and breakage phenomena in agitated wet granulation processes: a review. *Powder Technology*, 117:3–39, 2001. doi:10.1016/S0032-5910(01)00313-8.

[15] S. M. Iveson, P. A. L. Wauters, S. Forrest, J. D. Litster, G. M. H. Meesters, and B. Scarlett. Growth regime map for liquid-bound granules: further development and experimental validation. *Powder Technology*, 117:83–97, 2001. doi:10.1016/S0032-5910(01)00317-5.

[16] S. M. Iveson, J. A. Beathe, and N. W. Page. The dynamic strength of partially saturated powder compacts: the effect of liquid properties. *Powder Technology*, 127:149–161, 2002. doi:10.1016/S0032-5910(02)00118-3.

[17] P. C. Kapur and D. W. Fuerstenau. A coalescence model for granulation. *Industrial and Engineering Chemistry: Process Design and Development*, 8:56–62, 1969. doi:10.1021/i260029a010.

[18] B. F. C. Laurent. Structure of powder flow in a planetary mixer during wet-mass granulation. *Chemical Engineering Science*, 60:3805–3816, 2005. doi:10.1016/j.ces.2005.02.011.

[19] L. X. Liu, R. Smith, and J. D. Litster. Wet granule breakage in a breakage-only high shear mixer: Effect of formulation properties on breakage behaviour. In *Third International Granulation Workshop*, 2007.

[20] D. C. Montgomery and G. C. Runger. *Applied statistics and probability for engineers*. John Wiley & Sons, Inc., 3rd edition, 2003.

[21] Y. Muguruma, T. Tanaka, and Y. Tsuji. Numerical simulation of particulate flow with liquid bridge between particles (simulation of centrifugal tumbling granulator). *Powder Technology*, 109:49–57, 2000. doi:10.1016/S0032-5910(99)00226-0.

[22] A. M. Nilpawar, G. K. Reynolds, A. D. Salman, and M. J. Hounslow. Surface velocity measurement in a high shear mixer. *Chemical Engineering Science*, 61: 4172–4178, 2006. doi:10.1016/j.ces.2005.10.018.

[23] T. Schæfer. Growth mechanisms in melt agglomeration in high shear mixers. *Powder Technology*, 117:68–82, 2001. doi:10.1016/S0032-5910(01)00315-1.

[24] T. Simmons, R. Turton, and P. Mort. An investigation into the effects of time and shear rate on the spreading of liquids in coating and granulation processes. In *Fifth World Congress on Particle Technology*, 2006.

[25] J. Singh, M. Balthasar, M. Kraft, and W. Wagner. Stochastic modeling of soot particle size and age distributions in laminar premixed flames. *Proceedings of the Combustion Institute*, 30:1457–1465, 2005. doi:10.1016/j.proci.2004.08.120.

[26] J. Singh, R. I. A. Patterson, M. Kraft, and H. Wang. Numerical simulation and sensitivity analysis of detailed soot particle size distribution in laminar premixed ethylene flames. *Combustion and Flame*, 145:117–127, 2006. doi:10.1016/j.combustflame.2005.11.003.

[27] I. Talu, G. I. Tardos, and M. I. Khan. Computer simulation of wet granulation. *Powder Technology*, 110:59–75, 2000. doi:10.1016/S0032-5910(99)00268-5.

[28] G. I. Tardos, M. I. Khan, and P. R. Mort. Critical parameters and limiting conditions in binder granulation of fine powders. *Powder Technology*, 94:245–258, 1997. doi:10.1016/S0032-5910(97)03321-4.

[29] K. van den Dries, O. M. de Vegt, V. Girard, and H. Vromans. Granule breakage phenomena in a high shear mixer; influence of process and formulation variables and consequences on granule homogeneity. *Powder Technology*, 133:228–236, 2003. doi:10.1016/S0032-5910(03)00106-2.

[30] L. Vogel and W. Peukert. Breakage behaviour of different materials — construction of a mastercurve for breakage probability. *Powder Technology*, 129:101–110, 2003. doi:10.1016/S0032-5910(02)00217-6.

[31] D. Vojnovic, D. Chicco, and H. E. Zenary. Doehlert experimental design applied to optimization and quality control of a granulation process in a high shear mixer. *International Journal of Pharmaceutics*, 145:203–213, 1996. doi:10.1016/S0378-5173(96)04771-0.

[32] P. A. L. Wauters. *Modelling and mechanisms of granulation*. PhD thesis, Technische Universiteit Delft, 2001.